Auto-oxidation of Redox-Electrodes for the Selective Recovery of Platinum Group Metals

Journal:	*Journal of Materials Chemistry A*
Manuscript ID	TA-ART-02-2024-001384.R1
Article Type:	Paper
Date Submitted by the Author:	05-May-2024
Complete List of Authors:	Chung, Ching-Hsiu; University of Illinois Urbana-Champaign, chemical and biomolecular engineering Cotty, Stephen; University of Illinois at Urbana-Champaign, Chemical and Biomolecular Engineering Jeon, Jemin; University of Illinois at Urbana-Champaign, Chemical and Biomolecular Engineering Elbert, Johannes; University of Illinois at Urbana-Champaign, Chemical and Biomolecular Engineering Su, Xiao; University of Illinois at Urbana-Champaign, Chemical and Biomolecular Engineering

SCHOLARONE™
Manuscripts

ARTICLE

Auto-oxidation of Redox-Electrodes for the Selective Recovery of Platinum Group Metals

Ching-Hsiu Chung,[‡a] Stephen Cotty,[‡a] Jemin Jeon,[a] Johannes Elbert,[a] and Xiao Su*[a]

The recovery and purification of platinum group metals (PGMs) from multicomponent solutions is essential towards attaining a sustainable circular economy. Here, we design redox-active electrosorbents for the separation of PGM chloroanions, by leveraging the auto-oxidation of redox-electrodes. We synthesize a range of redox-metallopolymers with tunable redox potentials and demonstrate their molecular selectivity in multicomponent PGM mixtures. Iridium and platinum chloroanions were shown capable of simultaneous auto-oxidation and binding to the redox-polymers, spontaneously. Thus, due to the intrinsically high oxidation potential of the chloro-PGM complexes in leachate solutions, spontaneous electrochemical PGM recovery was possible without electrical or chemical input. As opposed to standard electrosorption, the energy consumption for iridium recovery is decreased by 75%. A combination of X-ray photoelectron spectroscopy (XPS) and ultraviolet-visible (UV-Vis) spectroscopy were used to track the auto-oxidation process of the redox-center and the iridium chloroanion. The redox potential of ferrocene polymers was found to affect the selectivity towards PGMs ions, with a high molecular selectivity achieved of over 100 between Pt and Rh. Using a porous-coated redox-polymer electrosorbent, over 186 mmol Pd uptake per mole of ferrocene moiety was achieved in the recovery of palladium from a catalytic converter leach solution. This work demonstrates an energy-efficient, process-intensified electrochemical platform for the multicomponent recovery of PGMs from waste feedstocks.

Introduction

Establishing a circular economy for PGMs is essential for the long-term sustainability of the energy industry, due to their core importance to the chemical and electrochemical industries.[1-4] PGMs have had widespread use in jewelry, automotive converter,[5] catalysts,[6, 7] pharmaceutical drugs,[8] and fuel cells,[9, 10] among others. The market price of PGMs has historically been on the rise, with Pd from $875 USD/oz in 2017 to $2,416 in 2021 (176% increasement) and Rh from $1,108 USD/oz in 2017 to $20,141 in 2021 (~17 times increasement) as shown in **Fig. 1a**.[11] Due to the similar physical and chemical properties between PGMs, separation is a significant challenge, with current industrial methods requiring several separation and purification processes[12, 13] (i.e., precipitation,[14] and solvent extraction).[15, 16] PGM mining requires significant of chemicals and energy input, and these demanding processes are fraught with pollution and environmental issues.[17] Therefore, effective recovery of PGMs is necessary and has high economical potential.

In both mining and catalytic converter recycling, strong oxidizers are a necessity to economically leach out PGMs into solution, thus the resulting PGM choro-complexes typically possess high oxidation states (**Fig. 1b**).[13, 18-21] However, hydrometallurgy and electrodeposition methods will fully reduce PGMs complexes to metallic PGMs, which is some form is wasting the potential energy of PGMs complexes.[13, 22] Furthermore, a large input of hydrochloric acid is necessary for PGMs leaching, which can be an issue due to the high energy consumption behind chloralkali electrolysis (>2000 kWh ton^{-1} Cl_2 generated).[23,24, 25] As a result, it is critical to develop an more energy efficient PGMs recovery process that better utilizes the oxidative potential of these valuable energetic complexes.

Electrosorption has been an attractive platform by applying specific potential or current to directly control the target ions capture/release, [26-30] combining low waste generation and nearly no chemical input.[31, 32] Recently, redox polymers have been extensively explored as a platform to enhance ion selectivity.[33, 34] Synthetic modulation of the functional groups of redox polymers can not only change the charge-transfer behavior[27, 35] but also provide new binding sites for target ions.[36] For instance, the electron donating groups next to ferrocene can tune the selectivity for heavy metal oxyanions electrosorption.[27] Recently, DFT studies have elucidated charge transfer as the core mechanism of ferrocene binding with platinum complexes.[37] However, the competitive electrosorption behavior between PGMs complexes is still unknown, which is critical to unlocking more efficient pathways to purifying PGMs, especially for sustainable mining.

Here, a reversible and spontaneous PGM adsorption system was accomplished with ferrocene polymers, by leveraging the auto-oxidation of redox couples for PGM recovery in waste recycling and mining contexts (**Fig. 1c**). We demonstrate that the chemical energy of high oxidation state PGMs complexes

a. Department of Chemical and Biomolecular Engineering, University of Illinois at Urbana-Champaign, IL 61801, United States

can be used for adsorption at the redox polymers, while significantly reducing the energy consumption through eliminating the energy cost of the forward electrosorption step. We also benchmark the tunable selectivity between PGMs through a combination of kinetic and equilibrium uptake studies for a range of ferrocene containing redox-polymers, including poly(vinyl ferrocene) (PVF), poly(3-ferrocenylpropyl methacrylamide) (PFPMAm), poly(2-((1-ferrocenylethyl)(methyl)amino)ethyl methacrylate) (PFEMA), and poly(2-(methacryloyloxy)ethyl ferrocenecarboxylate) (PFcMA) were investigated to understand the interaction with PGMs ions. Through tailored functional groups (amide, alkyl, amine, ester), the redox potential of these polymers were tuned, and as a result, their binding behavior and selectivity towards different PGMs. Moreover, X-ray photoelectron spectroscopy (XPS) and ultraviolet-visible (UV-Vis) spectroscopy were used to characterize the change in oxidation state of the PGMs complexes and redox polymers. Finally, to prove our applicability for practical PGM recovery, we applied our system

to the recovery of these critical elements from both mining and catalytic converter recycling contexts.

Results and discussion

Auto-oxidation of redox-couples and electrode characterization

To understand the redox properties of ferrocene polymers and PGMs ions, cyclic voltammetry of polyvinylferrocene-carbon nanotube (PVF-CNT) composites and PGMs ions were carried out. **Fig. 2a** showed that Ir(IV) can oxidize ferrocene polymers since the redox potential of PVF-CNT (370 mV vs Ag/AgCl) was lower than $[IrCl_6]^{2-}$ (the standard potential of $[IrCl_6]^{2-} + e^- \rightarrow [IrCl_6]^{3-}$ is 0.65 V versus Ag/AgCl). Therefore, if reduced PVF-CNT immersed in the $[IrCl_6]^{2-}$ solution, ferrocene will be oxidized to ferrocenium while $[IrCl_6]^{2-}$ will be reduced to $[IrCl_6]^{3-}$. This auto-oxidation behavior can be leveraged for PGM recovery through the spontaneous electrosorption and subsequent electrochemical release, thus requiring less energy input than a fully activated capture-and-release scheme (**Fig. 1b**).
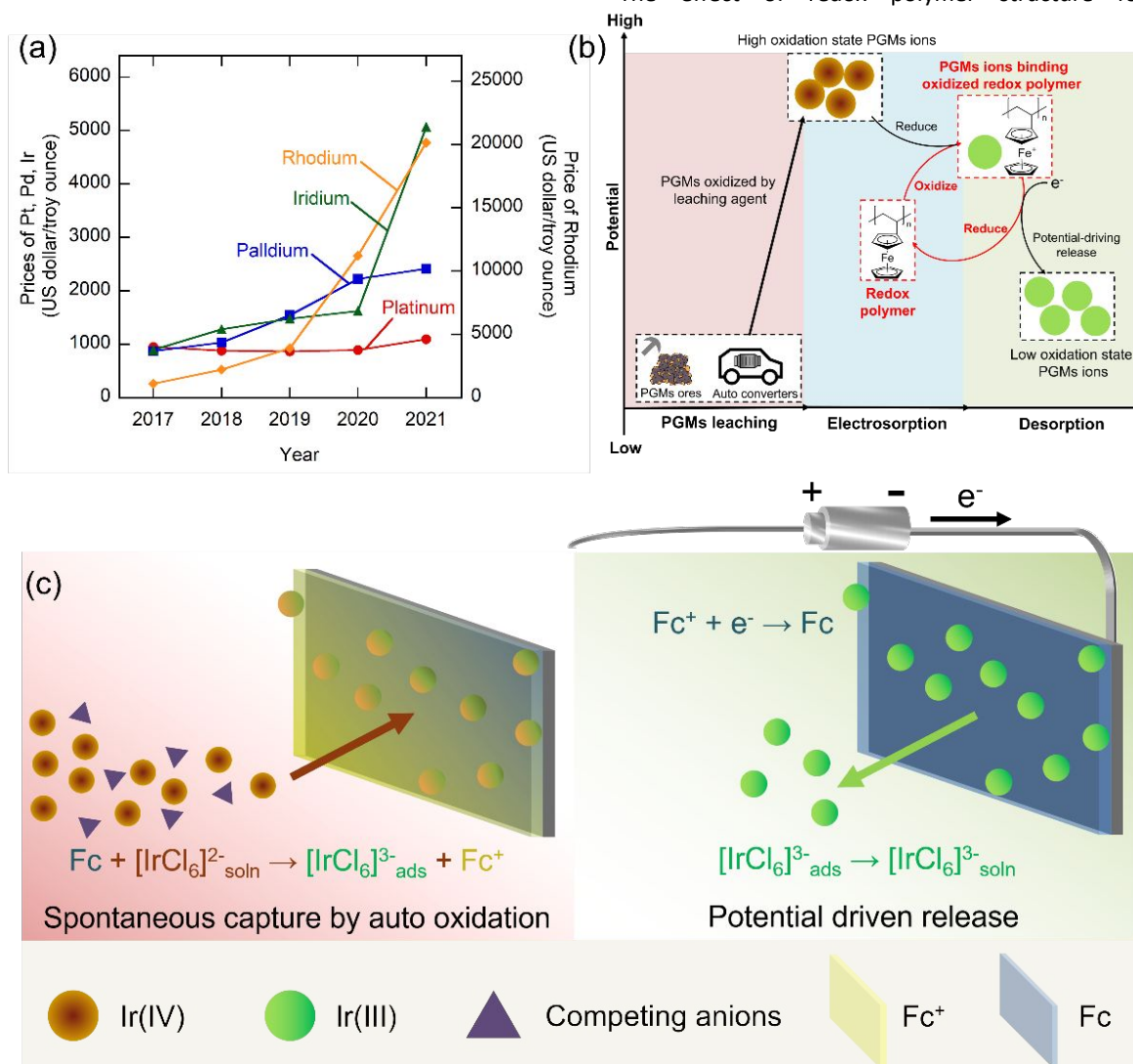
The effect of redox polymer structure for PGMs

Fig. 1 Market prices of PGMs and auto-oxidation adsorption and potential driven release between redox polymers for PGMs recovery. (a) Market prices of PGMs from 2017 to 2021 (Values reproduced from [11]). (b) Auto-oxidation of ferrocene and spontaneous adsorption of PGMs ions which have higher oxidation potential, and ferrocene regeneration with reducing potential applied. (c) $[IrCl_6]^{2-}$ auto-oxidized Ferrocene-based redox polymers and adsorbed on redox polymers as reduced form $[IrCl_6]^{3-}$ and oxidized redox polymers reduced by setting potential and released adsorbed $[IrCl_6]^{3-}$.

electrosorption was evaluated on PFPMAm, PVF, PFEMA, and PFcMA (**Fig. 2b**). The polymer synthesis followed published literature methods,[35, 38-40] with the detailed procedures and polymer characterization reported in the **ESI**. **Fig. 2b** presented the structure and measured redox potential of the redox polymers, and the cyclic voltammetry of redox polymers was shown in **Fig. S1** (**ESI**). **Fig. S2** (**ESI**) showed the scanning electron microscopy with energy dispersive X-ray spectroscopy (SEM-EDS) image of four redox polymers with carbon nanotubes coated on carbon paper, which demonstrated that all redox polymers were uniformly coated on the carbon paper. Among these four redox polymers, PFPMAm had the lowest redox potential (250 mV vs Ag/AgCl) followed by PVF (370 mV vs Ag/AgCl), PFEMA (490 mV vs Ag/AgCl), and PFcMA (600 mV vs Ag/AgCl). The potential difference between redox polymers was attributed to the electron donating and electron-withdrawing effects of the functional groups attached to the cyclopentadienyl.[41] The alkyl group of PFPMAm and PVF was electron donating, stabilizing the positive charge of ferrocenium (Fc$^+$), thus making ferrocene easier to oxidize.[27, 42] On the other hand, the amino methyl of PFEMA and the ester of PFcMA were electron withdrawing group, which increased the redox-potential of the ferrocene units by making them more difficult to oxidize.[38, 43, 44]

Structure effect of redox polymers for electrosorption

Iridium. To investigate the auto-oxidation behavior with four redox polymers, kinetic studies of uptake capacity with iridium (1 mM [IrCl$_6$]$^{2-}$ with 20 mM NaClO$_4$ as supporting electrolyte) at open circuit potential (OCP) were conducted. Iridium was selected as the model PGM for many of the studies due to its complementary redox potential to the metallopolymers, as well as its value and importance in the PGM industry. **Fig. 3a** showed that the adsorption uptake of iridium rapidly came to equilibrium within 15 minutes for PFEMA-CNT and PFcMA-CNT and reached equilibrium after 1 hour for all four polymers. PFPMAm-CNT had the highest 1-hour molar iridium adsorption uptake (388 mmol mol^{-1}), followed by PFEMA-CNT (284

mol^{-1}). The concentration profile of iridium in solution during the adsorption process was shown in **Fig. S3 (ESI).** The concentration of iridium dropped from 132 to 107 mg/L for PFPMAm-CNT, from 134 to 115 mg/L for PVF-CNT, from 123 to 107 mg/L for PFEMA-CNT, from 133 to 127 mg/L for PFcMA-CNT, while it remained 137 mg/L for CNT only. As for mass uptake per polymer loading, PFPMAm-CNT displayed the highest uptake (219 mg g^{-1}), followed by PVF-CNT (165 mg g^{-1}), PFEMA-CNT (155 mg g^{-1}), and PFcMA-CNT (43 mg g^{-1}). Uptake results revealed that PFPMAm-CNT has 38.8% utilization where 38.8% ferrocene of PFPMAm-CNT spontaneous bound to iridium. Adsorption with only CNT coated (0.2 mg) electrodes was carried out to prove that iridium uptake was driven primarily by the selective interactions of the redox polymer (**Fig. S4, ESI**). Compared with PVF-CNT (~80 mg/g-coating, 0.2 mg PVF and 0.2 mg CNT loading), the highest uptake with CNT was only 20 mg/g-coating, which was less than 25% of the iridium uptake with PVF-CNT. Therefore, the iridium uptake was mostly from the redox polymers. The profile of the potential of redox polymers (**Fig. 3b**) shows that the potential of redox polymers increased during iridium adsorption. while the potential of the CNT control electrode remained at ~0.8 V vs Ag/AgCl. Furthermore, **Fig. S5 (ESI)** showed that without H$_2$IrCl$_6$ (only supporting electrolyte NaClO$_4$), the potential of PVF-CNT can only increase to 340 mV vs Ag/AgCl, while with H$_2$IrCl$_6$ present, it increased to 652 mV vs Ag/AgCl. These results indicate that redox polymers were oxidized over time by [IrCl$_6$]$^{2-}$. In the meantime, the potential of counter electrode was decreasing (**Fig. S6, ESI**), suggesting that iridium in the solution was reducing (the counter electrode was bare carbon paper which will not react with the solution, so the potential of counter electrode can be seen as the potential of the solution) when exposed to redox polymer electrode. Therefore, the iridium was adsorbed via the auto-oxidation of the redox polymers and concurrent reduction of [IrCl$_6$]$^{2-}$ (**Fig. 3c**). Furthermore, **Fig. 3b** corresponded to the redox potential of redox polymers in standalone cyclic voltammetry with PFPMAm-CNT had the lowest open circuit potential at the beginning of iridium uptake (149 mV), followed by PVF-CNT (231 mV), PFEMA-CNT (251 mV), and PFcMA-CNT (411 mV). All potentials here are versus Ag/AgCl.
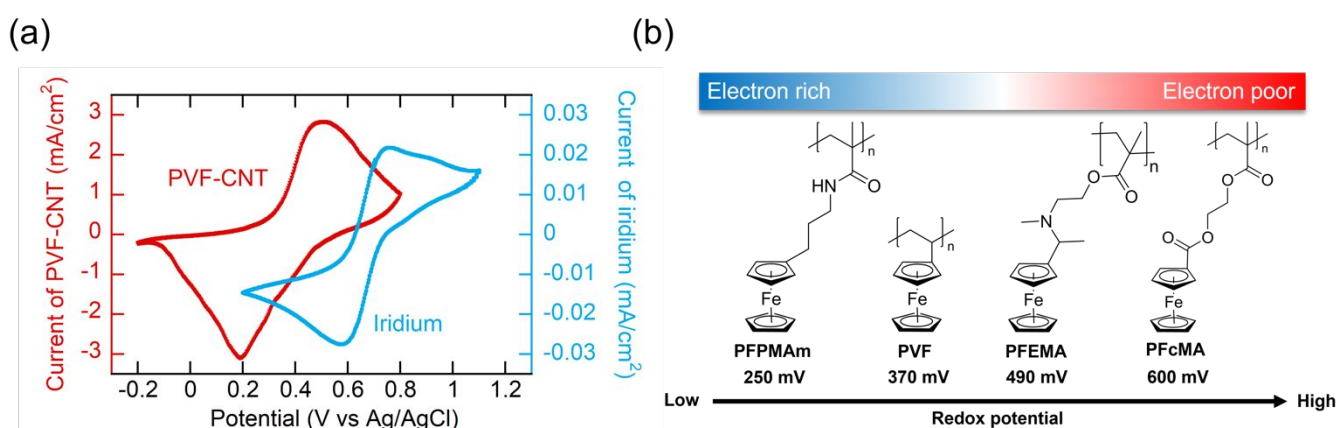
(a) (b)

Fig. 2 Redox potential and stucture of ferrocene redox polymers and redox potential of [IrCl$_6$]$^{2-}$. (a) Cyclic voltammetry comparing the redox-potentials of polyvinylferrocene (PVF) – carbon nanotube composite (PVF-CNT) *vs* iridium chloroanions (scan rate of 20 mV/s). The difference of the potential drives the spontaneous reaction between iridium and ferrocene. (b) Redox potentials and structures of PFPMAm, PVF, PFEMA, and PFcMA. Electrochemical potentials are presented vs Ag/AgCl.

mmol mol^{-1}), PVF-CNT (190 mmol mol^{-1}), and PFcMA-CNT (58 mmol

Platinum. The platinum ($[PtCl_6]^{2-}$) kinetic uptake at OCP with four redox polymers were also carried out and was similar to iridium, as shown in **Fig. S7 (ESI)**. PFPMAm-CNT had the highest uptake (491 mmol mol^{-1}) followed by PFEMA-CNT (348 mmol mol^{-1}), PVF-CNT (316 mmol mol^{-1}), and PFcMA-CNT (67 mmol mol^{-1}). The potential profile (**Fig. S7, ESI**) suggested that $[PtCl_6]^{2-}$ can auto-oxidize the reduced ferrocene redox polymers as well (the standard potential of $[PtCl_6]^{2-} + 2e^- \rightarrow [PtCl_4]^{2-} + 2Cl^-$ is 0.46 V versus Ag/AgCl). Notably, the reaction $[PtCl_6]^{2-} + 2e^- \rightarrow [PtCl_4]^{2-} + 2Cl^-$ was typically the intermediate reaction for platinum deposition ($[PtCl_4]^{2-} + 2 e^- \rightarrow Pt + 4 Cl^-$, E^o = 0.53 V vs Ag/AgCl). However, XPS results (**Fig. S8, ESI**) showed that the adsorbed platinum was only Pt(II) and Pt(IV), meaning there was no irreversible deposition of platinum on our electrosorption platform. Hence, the regeneration step was simpler using our electrosorption platform since Pt(II) was easier to be desorbed compared with deposited Pt.

In general, the adsorption uptake of PGMs ions was observed to increase with decreasing redox potential of the polymers (**Fig. 3d, S7**). PFPMAm-CNT had the highest uptake of iridium or platinum and lowest redox potential while PFcMA-CNT had the lowest uptake of iridium or platinum and highest redox potential. Therefore, PFPMAm-CNT had the largest driving force for electrosorption, originating from the highest potential difference with PGMs ions at OCP and resulting in more facile adsorption of PGM complexes. The difference of redox potential of redox polymers originated from their ferrocene neighboring functional groups.[41] Specifically, the electron donating group (alkyl group) of PFPMAm and PVF stabilized the positive charge of ferrocenium, making oxidation of the ferrocene and consecutive binding of PGMs anions easier.[27, 42] Nevertheless, the ester group of PFcMA is an electron withdrawing group, making

the reaction between PGM ions and ferrocene more difficult.[38, 43, 44] Interestingly, PFEMA-CNT had higher uptake of iridium (284 mmol mol^{-1}) than PVF-CNT (190 mmol mol^{-1}) even though its redox potential was higher (490 mV vs Ag/AgCl) than PVF-CNT (370 mV vs Ag/AgCl), as shown in **Fig. 3d**. The high uptake of iridium with PFEMA-CNT was caused by the methyl amino group of PFEMA-CNT functioning as an additional binding site for iridium adsorption (the nitrogen atom binds with Ir).[36, 45] Furthermore, from uptake profile in **Fig. 3a**, the first 2 minutes average adsorption rate of iridium with PFEMA-CNT (75.7 mmol mol^{-1} min^{-1}) was much faster than other redox polymers (17.0 mmol mol^{-1} min^{-1}). Moreover, from the kinetic adsorption fitting result (**Fig. S9, ESI**), only PFEMA-CNT was closer to seconder order adsorption while other three redox polymers were first order behavior.[46] The adsorption rate constant (k_{ads}) of PFEMA-CNT is 2.13 min^{-1}, which is 15 times higher than PFPMAm-CNT (0.074 min^{-1}), PVF-CNT (0.103 min^{-1}), and PFcMA-CNT (0.141 min^{-1}), implying that PFEMA had another adsorbing mechanism (methyl amino group provides additional binding sites)[36, 45] compared with other three redox polymers (charge transfer with ferrocene only).

Binary selectivity of PGMs ions during redox polymer electrosorption

To compare the performance redox polymers in multicomponent separations, selectivity maps of PGM uptakes in binary mixture were created (**Fig. 4a,b,c,d**). Binary PGM selectivity tests were carried out at OCP with 1:1 molar mixed 1 mM PGMs solution (0.5 mM for each PGMs ion) with 20 mM NaCl supporting electrolyte.

The binary ion-selectivity heatmaps for separation factors were obtained by using PVF-CNT, PFPMAm-CNT, PFEMA-CNT, and PFcMA-CNT at OCP for 1 hour adsorption with the PGMs ions at each row
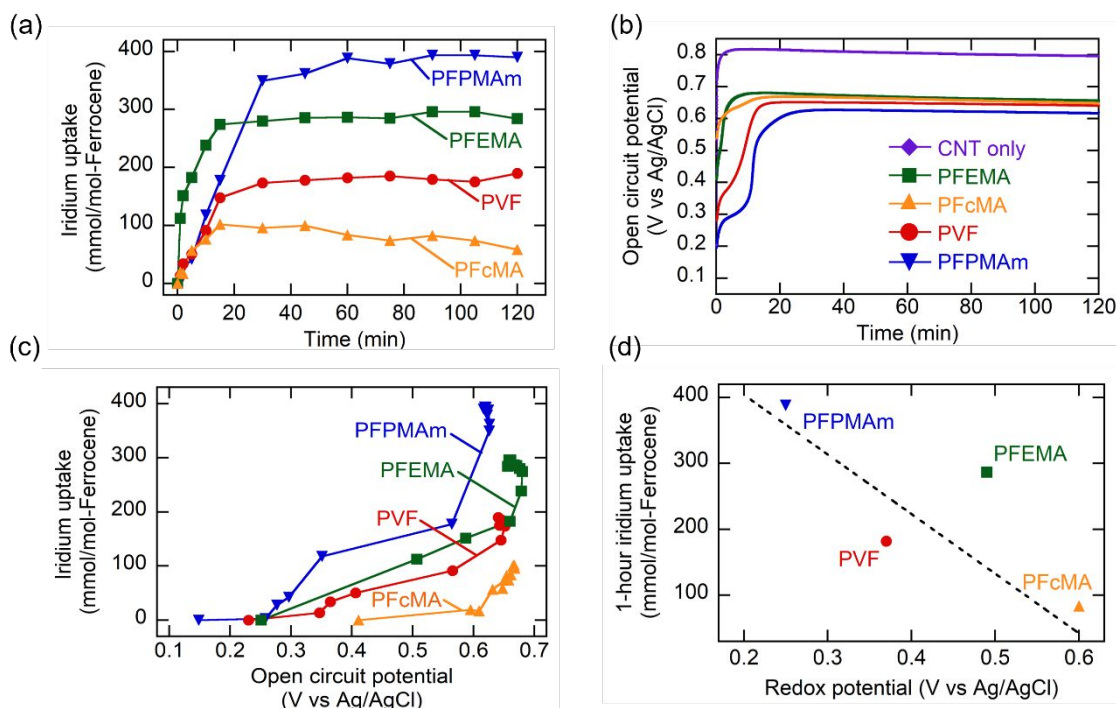

Fig. 3 1 mM H$_2$IrCl$_6$ electrosorption with ferrocene redox polymers-CNT (a) Iridium uptake profile of 1 mM H$_2$IrCl$_6$ (20 mM NaClO$_4$ as supporting electrolyte) with 0.4 mg redox polymers-CNT (0.2 mg redox polymer with 0.2 mg CNT) at OCP. (b) Potential profile of redox polymers-CNT and CNT control in 1 mM H$_2$IrCl$_6$ at OCP. (c) Relation between measured open circuit potential and iridium uptake in 1 mM H$_2$IrCl$_6$ with redox polymers-CNT at OCP. (d) Relation between 1-hour iridium uptakes of 1 mM H$_2$IrCl$_6$ with redox polymers-CNT and redox potentials of redox polymers-CNT, the regression line did not calculate PFEMA in.

labeled as species A and the PGMs ions at each column labeled as species B in separation factor $\alpha_{A, B}$. **Fig. 4a,b** showed that in binary PGMs solution, the binding preference of PFPMAm-CNT and PVF-CNT were Pt > Pd > Ru > Ir >> Rh while binding preference of PFEMA-CNT is Pd ≈ Pt > Ir > Ru >> Rh (**Fig. 4c**) and binding preference of PFcMA-CNT were Ir > Pd > Ru > Pt > Rh (**Fig. 4d**). The different selectivity between PGMs ions originates from the redox potential difference of the redox polymers. All four redox polymers had higher selectivity toward iridium in the $[IrCl_6]^{2-}/[RhCl_6]^{3-}$ mixture. While in $[PtCl_6]^{2-}/[RhCl_6]^{3-}$ mixtures, redox polymers had higher selectivity toward platinum except PFcMA-CNT, which had no uptake for both platinum and rhodium due to the high redox potential of PFcMA-CNT. This ion selectivity can be illustrated by the spontaneous reaction between redox polymers and $[PtCl_6]^{2-}$ or $[IrCl_6]^{2-}$, the auto-oxidation redox couple. $[PtCl_6]^{2-}$ or $[IrCl_6]^{2-}$ can auto oxidize the ferrocene moiety of redox polymers and bind with the oxidized ferrocene moiety of redox polymers after the charge transfer. However, there was no reaction between $[RhCl_6]^{3-}$ and the redox polymers at OCP, making $[PtCl_6]^{2-}$ and $[IrCl_6]^{2-}$ be adsorbed onto electrode easier compared with $[RhCl_6]^{3-}$, resulting in the difference in the adsorption uptake.

As for $[PtCl_6]^{2-}/[IrCl_6]^{2-}$ mixture, PFPMAm-CNT, PVF-CNT, and PFEMA-CNT showed higher selectivity toward platinum ($\alpha_{Pt, Ir}$ ranged from 1.17 to 1.54) while PFcMA-CNT showed higher selectivity toward iridium ($\alpha_{Pt, Ir}$ is 0.76). The difference of the selectivity originated from the different redox potential of redox polymers. In detail, PFcMA-CNT possessed the highest redox potential (0.6 V vs Ag/AgCl) and the standard reduction potential of $[PtCl_6]^{2-}$ (0.46 V vs Ag/AgCl) was smaller than the redox potential of PFcMA-CNT while the standard reduction potential of $[IrCl_6]^{2-}$ was 0.65 V vs Ag/AgCl, which was higher than the redox potential of PFcMA-CNT. Therefore, the interaction between $[IrCl_6]^{2-}$ and PFcMA-CNT will be more favorable compared with $[PtCl_6]^{2-}$. These results provided a guideline

for selective redox polymer design. We can design different electron donating/withdrawing group next to redox active sites of redox polymers to have specific redox potential for selective capturing PGMs anions. The high redox potential of PFcMA-CNT also illustrated why there was no uptake for platinum and rhodium in $[PtCl_6]^{2-}/[RhCl_6]^{3-}$ mixtures. The redox potential of PFcMA-CNT was higher compared to $[PtCl_6]^{2-}$.

For $[IrCl_6]^{2-}/[RuCl_5(NO)]^{2-}$ mixture, PFPMAm-CNT ($\alpha_{Ir, Ru}$ = 0.25) and PVF-CNT ($\alpha_{Ir, Ru}$ = 0.33) showed higher selectivity toward ruthenium while PFEMA-CNT ($\alpha_{Ir, Ru}$ = 1.46) and PFcMA-CNT ($\alpha_{Ir, Ru}$ = 1.73) showed the opposite trend, which can be attributed to PFEMA and PFcMA had higher redox potentials compared to PFPMAm and PVF. Therefore, PFEMA and PFcMA had higher selectivity of $[IrCl_6]^{2-}$ rather than $[RuCl_5(NO)]^{2-}$. After tracking the kinetics of adsorption (**Fig. 4e**), $\alpha_{Ir, Ru}$ decreased over time ($\alpha_{Ir, Ru}$ of PFEMA-CNT decreased from 1.77 at 30 minutes to 1.25 at 120 minutes and PFcMA-CNT decreased from 1.94 at 15 minutes to 1.56 at 120 minutes), which meant ferrocene redox polymers favored ruthenium rather than iridium as ferrocene was being oxidized (For PFcMA-CNT, the open circuit potential increased from 341 mV to 645 mV vs Ag/AgCl in 16 minutes and gradually decreased to 630 mV vs Ag/AgCl after 1 hour adsorption). The decrease of $\alpha_{Ir, Ru}$ over time was because $[IrCl_6]^{2-}$ worked as an oxidizer to oxidize the ferrocene during the OCP adsorption while the interaction between redox polymers and $[RuCl_5(NO)]^{2-}$ will be stronger once ferrocene being oxidized (In **Fig. 5a**, the uptake of ruthenium was five times at 0.8 V vs Ag/AgCl than at OCP). Furthermore, in **Fig. S10 (ESI)**, the uptake of iridium was decreasing after an hour OCP adsorption while the uptake of ruthenium increased, pointing to the ion-exchange between $[RuCl_5(NO)]^{2-}$ and $[IrCl_6]^{3-}$ over time as ferrocene was being oxidized, resulting in a dynamic $\alpha_{Ir, Ru}$ decreasing over time.

Separation factors under varying potentials (vs Ag/AgCl) were also evaluated. **Fig. 4f** summarized the separation factor of $[PtCl_6]^{2-}$
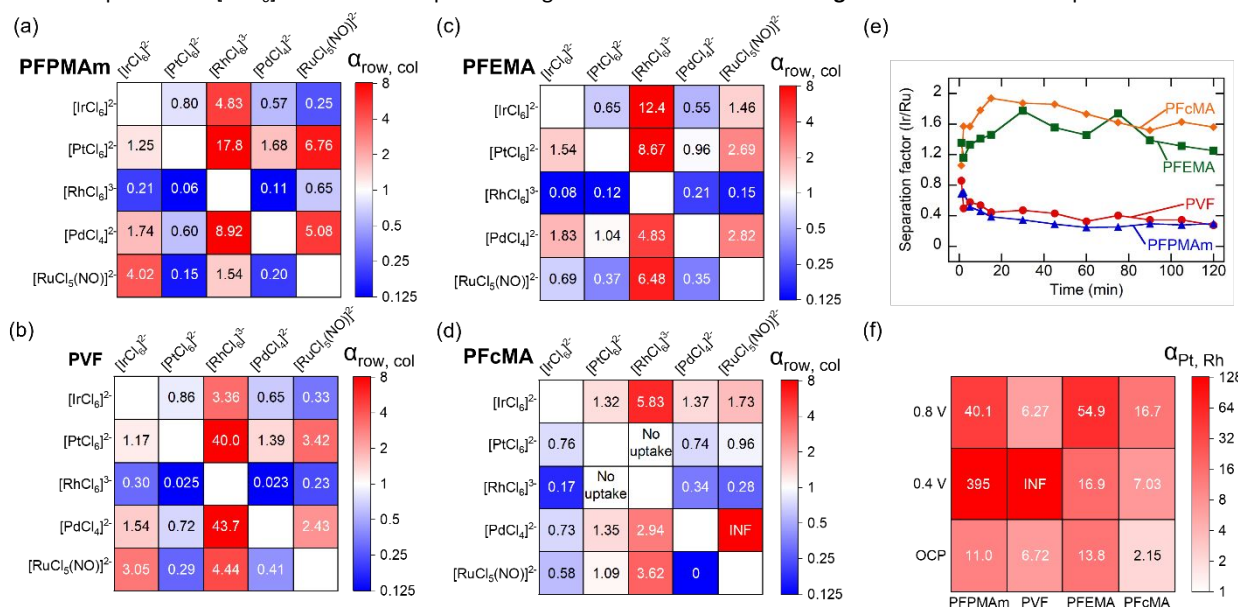

Fig. 4 Separation factor heat maps of 1-hour H_2IrCl_6, H_2PtCl_6, Na_3RhCl_6, K_2PdCl_4, $K_2RuCl_5(NO)$ binary mixtures (1 mM total PGMs (0.5 mM for each PGM ion) with 20 mM NaCl as supporting electrolyte) electrosorption at OCP with 0.4 mg (a) PFPMAm-CNT, (b) PVF-CNT, (c) PFEMA-CNT, (d) PFcMA-CNT, respectively (0.2 mg redox polymer with 0.2 mg CNT). The white color means separation factor is 1, INF means no uptake for the PGM ion in column. (e) Kinetic separation factor of $[IrCl_6]^{2-}$ over $[RuCl_5(NO)]^{2-}$ with redox polymers-CNT at open circuit potential adsorption. (f) Separation factor of $[PtCl_6]^{2-}$ over $[RhCl_6]^{3-}$ in H_2PtCl_6 and Na_3RhCl_6 binary mixture with 20 mM $NaClO_4$ supporting electrolyte for 1-hour electrosorption with redox polymers-CNT at open circuit potential or 0.4 V, 0.8 V versus Ag/AgCl.

over [RhCl$_6$]$^{3-}$ at OCP, 0.4 V and 0.8 V vs Ag/AgCl with all four redox polymers. For PVF-CNT and PFPMAm-CNT, $\alpha_{Pt, Rh}$ reached maximum at 0.4 V (infinite (no Rh uptake) for PVF-CNT, 395 for PFPMAm-CNT) while $\alpha_{Pt, Rh}$ of PFEMA-CNT and PFcMA-CNT increased as applied potential increased. $\alpha_{Pt, Rh}$ of PFEMA-CNT increased from 13.8 (OCP) to 16.9 (0.4 V) and 54.9 (0.8 V), and $\alpha_{Pt, Rh}$ of PFcMA-CNT increased from 2.15 (OCP) to 7.03 (0.4 V) and 16.7 (0.8 V). The change of $\alpha_{Pt, Rh}$ at different applied potential can be explained by the redox potential of redox polymers. The redox potential of PFPMAm-CNT (250 mV vs Ag/AgCl) and PVF-CNT (370 mV vs Ag/AgCl) was lower than 0.4 V while redox potential of PFEMA-CNT (490 mV vs Ag/AgCl) and PFcMA-CNT (600 mV vs Ag/AgCl) was higher than 0.4 V, resulting in PFPMAm-CNT and PVF-CNT being oxidized at 0.4 V vs Ag/AgCl while PFEMA-CNT and PFcMA-CNT being reduced. Furthermore, **Fig. 5a** showed that there was no uptake of rhodium at OCP, indicating oxidation of ferrocene was necessary for rhodium electrosorption Therefore, for PFPMAm-CNT and PVF-CNT, though 0.4 V vs Ag/AgCl oxidize the ferrocene, it was limited to 0.4 V which was lower than the potential at 60 minutes OCP adsorption (0.54 V vs Ag/AgCl for PFPMAm-CNT, 0.51 V vs Ag/AgCl for PVF-CNT), limiting the driving force for rhodium adsorption while no significant effect for platinum. Hence, $\alpha_{Pt, Rh}$ reached maximum when 0.4 V vs Ag/AgCl was applied. However, at 0.8 V vs Ag/AgCl, the uptake of platinum and rhodium was enhanced (uptake of platinum increased by 3 times compared to 0.4 V vs ag/AgCl applied while rhodium from no uptake to 47 mmol mol^{-1} with PVF-CNT), making the adsorption between [PtCl$_6$]$^{2-}$ and [RhCl$_6$]$^{3-}$ comparable. As a result, $\alpha_{Pt, Rh}$ decreased at 0.8 V vs Ag/AgCl compared to 0.4 V vs Ag/AgCl. As for PFEMA-CNT and PFcMA-CNT, applying a 0.4 V vs Ag/AgCl reduced both polymers, thus limiting the adsorption of [PtCl$_6$]$^{2-}$. Moreover, as applied potential increased, uptake of [PtCl$_6$]$^{2-}$ and [RhCl$_6$]$^{3-}$ will be enhanced, especially for [PtCl$_6$]$^{2-}$ (uptake of platinum increased by 4 times compared to 0.4 V vs Ag/AgCl applied while uptake of rhodium increased by 1.8 times). Hence, $\alpha_{Pt, Rh}$ increased as applied potential increased. **Fig. 4f** indicated the close relation of operating potential and redox potential with adsorption selectivity.

Separation performance of redox electrodes towards PGMs

Single-PGM electrosorption performance. First, the adsorption of PVF-CNT towards each individual PGM was investigated in model solutions containing 1 mM of one PGMs ion salt (H$_2$IrCl$_6$, H$_2$PtCl$_6$, Na$_3$RhCl$_6$, K$_2$PdCl$_4$, K$_2$RuCl$_5$NO) and 20 mM sodium perchlorate (NaClO$_4$) or sodium chloride (NaCl) supporting electrolytes in DI water. For the desorption and regeneration, adsorbed species were released in 20 mM sodium perchlorate at 0.2 V vs Ag/AgCl applied potential. All PGMs solutions here were acidic and H$_2$PtCl$_6$ had the lowest pH value (2.3), followed by H$_2$IrCl$_6$ (2.9), K$_2$PdCl$_4$ (3.0), K$_2$RuCl$_5$NO (3.3), and Na$_3$RhCl$_6$ (4.8). The uptake and regeneration efficiency of PGMs ions with PVF-CNT (**Fig. 5a**) showed that PVF-CNT had an uptake (with unit in mmol PGMs per mol ferrocene moiety) of 163 for iridium, 197 for platinum, 6.7 for rhodium, 180 for palladium, and 41 for ruthenium at OCP for an hour and had high regeneration efficiency with iridium (79%) and ruthenium (81%) after 1 hour desorption. **Fig. 5c,d,e** showed the SEM-EDS images of iridium on PVF-CNT coated electrode, confirming the adsorption and release of iridium. Notably, the regeneration efficiency of palladium was around zero, implying that palladium is deposited on redox polymers

after adsorption, which there were some Pd nanoparticles on the surface of the electrode (**Fig. S11**, **ESI**).

To enhance the electrosorption performance, potential was applied to oxidize PVF-CNT. In **Fig. 5a**, after applying 0.8 V vs Ag/AgCl, the uptake was increased by 38% for iridium, 18% for platinum, 1125% for rhodium, and 149% for ruthenium. Platinum showed the highest uptake (252 mmol mol^{-1}) followed by iridium, ruthenium, and rhodium (249, 216, 170 mmol mol^{-1}, respectively). Furthermore, the regeneration efficiency did not decrease, and was 92% for iridium, 83% for ruthenium, 58% for rhodium, and 54% for platinum.

Tracking oxidation state of redox electrode. Fe 2p and Ir 4f XPS results (reference to C-C C1s at 284.8 eV) illustrated the charge transfer binding mechanism that before adsorption, as shown in **Fig. 5f**, the Fe 2p displayed strong spin-orbiting of 2p$_{3/2}$ and 2p$_{1/2}$ at binding energy 707.7 eV and 720.5 eV for unoxidized ferrocene respectively, meaning that the prepared PVF-CNT electrode only had reduced form (Fc).[47] Nevertheless, after adsorption with iridium, the signal of Fe 2p$_{3/2}$ and 2p$_{1/2}$ transition at 707.7 eV and 720.5 eV decreased and new peaks generated at 709.9 eV and 723.1 eV, indicating that ferrocene was oxidized (Fc -> Fc$^+$ + e$^-$), as shown in **Fig. 5g**. These results agreed with the previously reported Fc$^+$ binding energies.[48] Specifically, 82.8% of ferrocene in the PVF-CNT got oxidized after 1-hour [IrCl$_6$]$^{2-}$ adsorption at OCP. The peaks of Ir 4f$_{7/2}$ and Ir 4f$_{5/2}$ displayed at binding energy 61.9 eV and 64.9 eV respectively.[49] The quantitative deconvolution of Ir 4f$_{5/2}$ and Ir 4f$_{7/2}$ was carried out by using H$_2$Ir(IV)Cl$_6$ and K$_3$Ir(III)Cl$_6$ standards (**Fig. 5i,j**). Binding energies at 61.8 eV and 64.7 eV were assigned to Ir(III) while binding energies at 62.8 eV and 65.8 eV were specified as Ir(IV). **Fig. 5l** showed the Ir 4f XPS spectra of PVF-CNT after 1-hour iridium adsorption at OCP, and the deconvolution results showed that there was no Ir(IV) but only Ir(III) on PVF-CNT, indicating that during H$_2$Ir(IV)Cl$_6$ adsorption, Ir(IV) in the solution got reduced by ferrocene and became Ir(III) to bind with PVF-CNT ([IrCl$_6$]$^{2-}$ + Fc -> [IrCl$_6$]$^{3-}$Fc$^+$). When a reducing potential (0.2 V vs Ag/AgCl) was applied to regenerate, ferrocenium was reduced back to ferrocene and released Ir(III) at the same time, where no iridium was deposited (**Fig. 1c, 5m**).

Tracking oxidation state of PGMs ions in solution. The UV-Vis spectra (**Fig. S12, ESI**) of the releasing solution showed no Ir(IV), indicating that all the released iridium was Ir(III),[50] which corresponded to the XPS results. Therefore, we proposed the binding mechanism between [IrCl$_6$]$^{2-}$ or [PtCl$_6$]$^{2-}$ and PVF-CNT was from the reduction-oxidation reaction of ferrocene and PGM ions (**Fig. 1c**). The kinetic release of iridium with PVF-CNT at 0.2 V versus Ag/AgCl (**Fig. S13**, **ESI**) showed that the release of iridium reached equilibrium after 10 minutes. The multiple adsorption and release cycles of H$_2$IrCl$_6$ with PVF-CNT (**Fig. S14, ESI**) showed that the uptake of iridium was stable at first three cycles (around 140 mmol mol^{-1}), with some of the ferrocene units of PVF-CNT staying in the oxidized form after 0.2 V versus Ag/AgCl applied, as shown in **Fig. 5h**. Furthermore, SEM-EDS and XPS results indicated some iridium residue on the electrodes after desorption (**Fig. 5e, m**), limiting the uptake for

next adsorption. Therefore, the uptake dropped slightly over cycles. However, the regeneration efficiency of each cycle was over 90%, indicating that there was no significant loss in capacity and that the redox-metallopolymers can be reusable adsorbents for PGMs ions.

To justify our hypothesis for binding mechanism, 1 mM $K_3Ir(III)Cl_6$ electrosorption tests with PVF-CNT were conducted (**Fig. 5b**). Compared with $[Ir(IV)Cl_6]^{2-}$, the uptake of $[Ir(III)Cl_6]^{3-}$ was significantly lower at OCP (43 mmol mol^{-1}, **Fig. S15a**, **ESI**), and the potential profile of $[IrCl_6]^{3-}$ electrosorption only raised

from 250 mV to 350 mV versus Ag/AgCl after an hour at OCP (**Fig. S15b**, **ESI**), which meant ferrocene was only oxidized slightly. However, the uptake of $[IrCl_6]^{3-}$ when 0.8 V versus Ag/AgCl applied was 3.5 times than at OCP and comparable to the uptake of oxidized $[IrCl_6]^{2-}$ at OCP, indicating the oxidation of ferrocene is essential for the electrosorption of iridium. Therefore, we proposed that the oxidation state of PGMs ions affected the electrosorption behavior of ferrocene redox polymers in a way that PGMs ions which can auto-oxidize ferrocene had higher uptake.
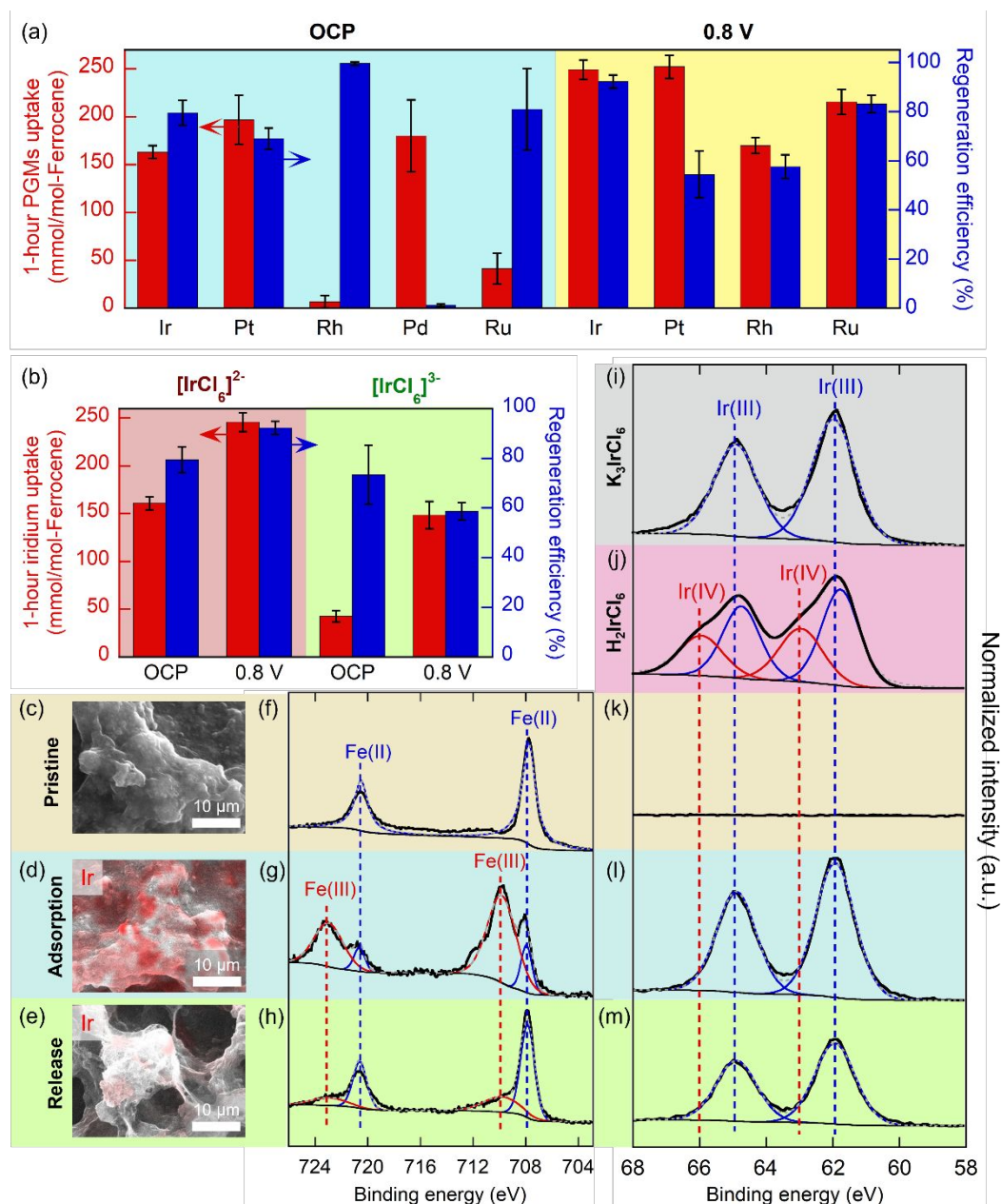

Fig. 5 (a) 1-hour PGMs uptake (1 mM PGMs ions with 20 mM NaClO$_4$ as supporting electrolyte) with 0.4 mg PVF-CNT (0.2 mg PVF and 0.2 mg CNT) at OCP or 0.8 V versus Ag/AgCl and regeneration efficiency of PVF-CNT at 0.2 V versus Ag/AgCl desorption for an hour in 20 mM NaClO$_4$. (Ir: H$_2$IrCl$_6$, Pt: H$_2$PtCl$_6$, Rh: Na$_3$RhCl$_6$, Ru: K$_2$RuCl$_5$(NO), *Palladium adsorption was tested in 1 mM K$_2$PdCl$_4$ with 20 mM NaCl supporting electrolyte). (b) 1-hour iridium uptake and regeneration efficiency of different valent of iridium with PVF-CNT at OCP or 0.8 V versus Ag/AgCl (1 mM iridium chloroanions with 20 mM NaClO$_4$ as supporting electrolyte) with 0.4 mg PVF-CNT. (c), (d), (e) SEM images and EDS mapping of PVF-CNT before and after 1-hour H$_2$IrCl$_6$ adsorption at OCP, and after 1-hour 0.2 V versus Ag/AgCl desorption. (f), (g), (h), Fe 2p XPS of PVF-CNT before and after 1-hour H$_2$IrCl$_6$ adsorption at OCP, and after 1-hour 0.2 V versus Ag/AgCl desorption. (i), (j) Ir 4f XPS of dried 1 mM K$_3$IrCl$_6$ or H$_2$IrCl$_6$ aqueous solution on carbon paper. (k), (l), (m) Ir 4f XPS of PVF-CNT before and after 1-hour H$_2$IrCl$_6$ adsorption at OCP, and after 1-hour 0.2 V versus Ag/AgCl desorption.

To further understand the spontaneous reaction between PGMs ions and redox polymers, electrochemical quartz crystal microbalance () measurements were carried out. EQCM can determine the mass change of the electrode by measuring the frequency changes under potential control.[51-53] In **Fig. S16** and **Fig. S17** (**ESI**), the mass of the working electrode with PVF coating was increasing as the potential of PVF was rising during OCP electrosorption, which meant $[PtCl_6]^{2-}$ and $[IrCl_6]^{2-}$ spontaneously oxidize PVF and be adsorbed, same as the result we got in kinetic electrosorption tests (**Fig. 3a,b** and **Fig. S7**). **Fig. S17** showed three uptake and release cycles (uptake: OCP for 1 hour, release: 0.2 V versus Ag/AgCl for 10 minutes) of $[PtCl_6]^{2-}$ with PVF, indicating that PVF can release adsorbed $[PtCl_6]^{2-}$ back into solution when 0.2 V versus Ag/AgCl potential was applied. Furthermore, the plot of the mass change of PVF coating electrode versus potential for $[IrCl_6]^{2-}$ adsorption (**Fig. S16**, **ESI**) were classic Nernstian behavior, indicating that $[IrCl_6]^{2-}$ were adsorbed onto PVF right after the charge transfer,[54] which corresponded to the XPS results.

Mass loading effect of electrodes. The mass loading of electrode materials can be critical to their practical applications.[55] To optimize the redox polymer loading for electrosorption, different mass loadings (0.2, 0.4, 1, 2, 4, unit in mg-PVF/cm²) of PVF-CNT (1:1 in mass ratio) were tested for iridium adsorption at OCP and 0.8 V vs Ag/AgCl applied potential, as shown in **Fig. S18 (ESI)**. **Fig. S18a** showed that at 0.8 V vs Ag/AgCl applied potential, the total uptake of iridium can be enhanced up to 90.4 μg when using 1.0 mg/cm² PVF loading, which was 97% more than the total uptake of 0.2 mg PVF loading. However, the ferrocene stoichiometric utilization decreased by 60% at these higher loadings, indicating that the iridium uptake did not increase with the PVF loading linearly.

The adsorption by auto-oxidation is limited mostly at the surface of the polymers, with mass-transfer limitations at higher loadings which limit spontaneous charging, which can be seen by the lower open circuit potential at higher mass loadings of ferrocene (**Fig. S18b**). Compared with 0.2 mg cm⁻² PVF loading (652 mV vs Ag/AgCl), the OCP of 0.4 mg cm⁻² PVF was only 527 mV vs Ag/AgCl after 1-hour iridium adsorption, followed by 1.0 mg cm⁻² PVF (409 mV vs Ag/AgCl), 2.0 mg cm⁻² PVF (375 mV vs Ag/AgCl), 4.0 mg cm⁻² PVF (362 mV vs Ag/AgCl). At the same time, the iridium uptake increased by 3 times by applying 0.8 V vs Ag/AgCl compared to OCP for iridium adsorption, due to the higher fraction of ferrocene oxidized. As such, at higher redox polymer loadings, applying potential to oxidize the electrodes or better dispersion of redox polymers are critical to enhancing the redox-mediated adsorption of the PGMs chloroanions.

Recovery of PGMs from simulated mining streams and recycling of catalytic converter

Hydrochloric acid is commonly used in PGMs mining industry to leach PGMs from the ores,[13] and chloride (Cl^-) has been reported to degrade ferrocenium,[56] as also shown in **Fig. S19 (ESI)**. 20 mM sodium chloride or hydrochloric acid were used as supporting electrolyte to test the effect of chloride for PGMs ions electrosorption with PVF-CNT. Results showed that OCP operation with PVF-CNT was applicable in chloride existing solution (**Fig. S20**, **ESI**). In fact, as shown in **Fig. S20a (ESI)**, iridium can be adsorbed by PVF-CNT in 20 mM sodium chloride where the uptake of iridium was 466 mmol mol⁻¹ ferrocene, even higher than the uptake of iridium in 20 mM sodium perchlorate (312 mmol mol⁻¹ ferrocene). Furthermore, the regeneration efficiency of PVF-CNT after iridium electrosorption in 20 mM sodium chloride remained same as electrosorption in 20 mM sodium perchlorate (>80%), shown in **Fig. S20b (ESI)**. As for hydrochloric acid, the uptake of iridium in 20 mM hydrochloric acid was 395 mmol mol⁻¹ ferrocene, demonstrating that PVF-CNT can be used for iridium electrosorption at OCP in acidic
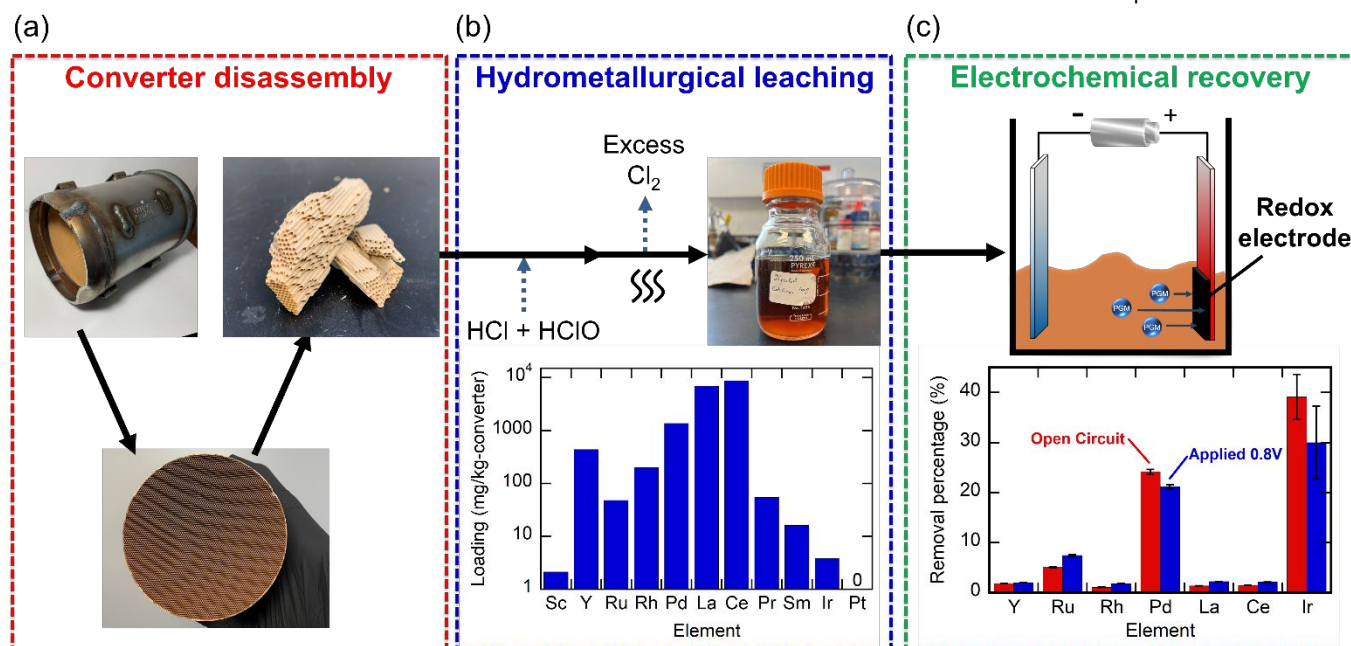

Fig. 6 PGM recycling from catalytic converters using redox-mediated electrosorption. (a) Catalytic converter (2014 Scion Tc was purchased new from Toyota) disassemble and digested by HCl and HClO. (b) Element composition of catalytic converter digested by HCl and HClO. (c) Electrochemical recovery platform and remove percentage of PGMs and other elements at open circuit potential or 0.8 V applied potential versus Ag/AgCl with PVF-CNT from leach catalytic converter.

chloride existing environment. However, because of the high acidic environment from hydrochloric acid, the regeneration efficiency of PVF-CNT after iridium adsorption in 20 mM hydrochloric acid was only 70% (**Fig. S20b, ESI**). We observed that the PVF-CNT was not leached by Cl^- because during the iridium adsorption at OCP, $[IrCl_6]^{2-}$ simultaneously oxidized ferrocene and became $[IrCl_6]^{3-}$ to bind to ferrocenium right after the charge transfer – thus resulting in high selectivity towards iridium chloroanions over Cl^-. These results demonstrated that redox polymers have the potential to be applied in PGMs mining industry using auto-oxidation redox couple in chloride media.

To demonstrate real-world applicability, our PVF-CNT electrosorption system was used to selectively capture PGMs from an automotive catalytic converter (Toyota 2014 Scion Tc). The catalytic converter was crushed into small pieces and leached with HCl and HClO, forming an aqueous leach solution containing 51.44 ppm Pd, 7.47 ppm Rh, 1.98 ppm Ru, and 0.23 ppm Ir (**Fig. 6b, Table S1**). Adsorption with PVF-CNT electrodes were carried out directly in the leach solution at OCP, and with an applied 0.8 V versus Ag/AgCl. Pd yielded the highest molar uptake at 186 mmol mol^{-1}. Despite the low concentration of iridium in the leach solution (0.23 ppm), PVF-CNT electrodes were able to adsorb 30.0% of iridium with an applied potential of 0.8 V, and 39.1% of iridium was adsorbed from the leach solution with no applied potential (OCP), shown in **Fig. 6c.**

Uptake performance was similar between OCP and applied potential experiments for all elements tested, shown in **Fig. 6c**. However, compared with 0.8 V vs Ag/AgCl applied potential, removal of Pd was enhanced at OCP by 14% and Ir was enhanced at OCP by 30%. Similar to previous results, the measured potential response of the open circuit adsorption experiment suggested that initially reduced ferrocene sites on the electrode surface were progressively oxidized, going from an initial potential of 0.28 V to 0.38 V (**Fig. S21, ESI**), and the leach solution was simultaneously reduced, shown as a decrease in potential from 0.86 V to 0.5 V, indicating that the PVF-CNT electrode was oxidized by the leach solution spontaneously without any energy input. Comparatively, when a constant 0.8 V vs Ag/AgCl was applied to the PVF-CNT electrode, 150 J/g-PVF of energy was consumed to oxidize the PVF-CNT electrode in the catalytic converter leach solution (**Fig. S22, ESI**). Our results showed that PVF-CNT electrodes resulted in selective and energy efficient capture of PGMs from catalytic converter leach solution.

Energy consumption of PGMs adsorption with PVF-CNT

In conventional hydrometallurgical methods, the chemical energy from PGM ions is not utilized and lost since it uses chemicals to fully reduce PGMs.[13] However, auto-oxidation redox couple utilized the wasted chemical energy of PGMs (oxidizing potential) for selective capture while simultaneously reconstitute the oxidizing leachates during PGMs release, cutting down the energy cost since no extra was needed in the adsorption step. Specifically, only the electrochemical desorption step required energy input, as the adsorption step leveraged the auto-oxidation and redox-couples to spontaneously adsorb chloroanions. **Fig. 7** showed the energy consumption of the processes when comparing OCP or 0.8 V vs Ag/AgCl adsorption, coupled 0.2 V vs Ag/AgCl desorption with PVF-CNT. Results showed that though the energy consumption of desorption is slightly higher after OCP adsorption compared to 0.8 V adsorption, OCP adsorption did not need energy input in adsorption

step that in total OCP adsorption can save around 75% for Ir recovery, 68% for Rh recovery, and 20% for Pt recovery compared to 0.8 V adsorption. These results indicated that OCP adsorption of PGMs complexes with ferrocene polymers was a significantly more energy effective method compared with applying potential.

Energy saving with PVF-CNT in chloralkali electrolysis

To prove adsorption with redox polymers is more energy efficient compared to traditional hydrometallurgy processes, pre-oxidized PVF-CNT electrode in chloralkali electrolysis was carried out. Results showed that using pre-oxidized PVF-CNT coated carbon paper as cathode can save 50% of the energy consumption compared to using carbon paper without redox polymers (**Fig. S23, ESI**). Specifically, in **Fig. S24a (ESI)**, the traditional chloralkali electrolysis generates hydrogen at cathode (-0.8 V vs Ag/AgCl), which needed more potential applied compared to the reduction of PVF-CNT (0.4 V vs Ag/AgCl) while same potential at the anode for generating chlorine (1.36 V vs Ag/AgCl). Therefore, the overall cell potential of chloralkali electrolysis by using carbon paper as cathode (generating hydrogen) will be two times of using PVF-CNT as cathode (reducing ferrocene), as shown in **Fig. S24b (ESI)**. Combining the desorption step and chloralkali electrolysis, it can not only save the energy by 49% for generating chloride for PGMs leaching, but also reduce PVF-CNT to
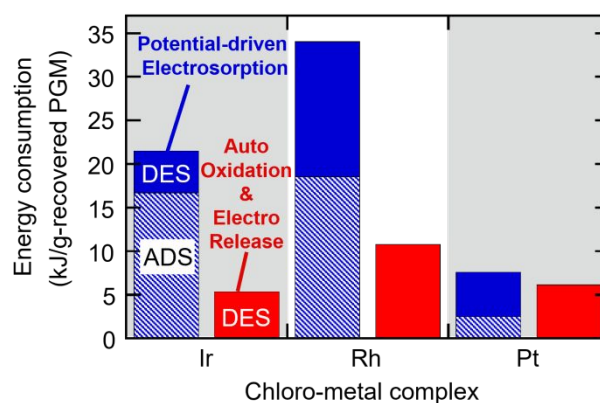

Fig. 7 Energy consumption of PGMs complexes with PVF-CNT at OCP or 0.8 V vs Ag/AgCl adsorption and 0.2 V vs Ag/AgCl desorption.

release the adsorbates. Hence, a more energy-efficient chloralkali electrolysis process was invented by recyclable adsorbent PVF-CNT.

Conclusion

Our study demonstrated the energy efficient recovery of PGMs through the synthetic tuning of redox-metallopolymers, to leverage the auto-oxidation between the redox-active electrode and the redox-active PGM chloroanions for spontaneous capture. Ferrocene-based redox polymers was shown to auto-oxidize in the presence of $[IrCl_6]^{2-}$ or $[PtCl_6]^{2-}$, thus promoting the spontaneous and selective PGM chloroanion adsorption. The platform was applied to the recycling of valuable elements from waste catalytic converters, through the leaching and electrochemical recovery of the PGMs. The energy consumption with the application of auto-oxidation redox couple (5.3 kJ g^{-1}) decrease by 75% compared to electrosorption at 0.8 V vs Ag/AgCl (21.5 kJ g^{-1}) for Ir recovery. Tuning the polymer structure was shown to be able to modulate

the selectivity and uptake of PGMs chloroanions. Remarkably, PFcMA-CNT showed selectivity for $[IrCl_6]^{2-}$ over $[RuCl_5(NO)]^{2-}$ and $[IrCl_6]^{2-}$ over $[PtCl_6]^{2-}$ while PFPMAm-CNT and PVF-CNT showed reverse selectivity in the binary competitive adsorption at open circuit potential. The separation factor of $[PtCl_6]^{2-}$ over $[RhCl_6]^{3-}$ was the highest which can be up to 40 at open circuit potential and raised to over 100 at 0.4 V vs Ag/AgCl. PFPMAm-CNT had the highest Ir uptake (388 mmol mol^{-1}) because of the lowest redox potential. Amino methyl group of PFEMA can be an additional adsorption site, resulting in the high Ir uptake (284 mmol mol^{-1}) even though the redox potential of PFEMA-CNT is high (490 mV vs Ag/AgCl). For real world application, ferrocene-based redox polymer can be used for recovering PGMs from automotive converter leaching streams (186 mmol Pd uptake per mole of ferrocene moiety). The auto-oxidation based binding mechanism was tracked through a combination of electrosorption and spectroscopy. Fe 2p XPS showed that ferrocene of redox polymer was oxidized after adsorption in $[IrCl_6]^{2-}$ solution, and Ir 4f XPS displayed that $[IrCl_6]^{2-}$ can oxidize ferrocene and become $[IrCl_6]^{3-}$ to bind with PVF-CNT. In summary, our work presents a promising electrochemical PGMs recovery system with less energy input that can facilitate the adsorption of PGMs ions by the potential difference and control the selectivity between PGMs ions by modifying the applied potential or the polymer structure. We envision the system can be applied in industry after process optimization and improving the separation factor and regeneration efficiency by inventing new redox polymers with better performance.

Experimental

Materials and Synthesis

All chemicals were obtained from Sigma Aldrich, Fisher Scientific or Polysciences Inc, and used as received. poly(3-ferrocenylpropyl .methacrylamide) (PFPMAm), poly(2-((1-ferrocenylethyl)(methyl)amino)ethyl methacrylate) (PFEMA), and poly(2-(methacryloyloxy)ethyl ferrocenecarboxylate) (PFcMA) were synthesized as reported previously (ESI†).[35, 38-40] All Nanostructured redox polymer/carbon nanotubes electrodes (PVF-CNT, PFPMAm-CNT, PFEMA-CNT, and PFcMA-CNT) were made by drop casting of a polymer ink solution (redox polymer mixed with carbon nanotube in 1:1 mass ratio in chloroform solution).[37] The addition of carbon nanotubes (CNT) is to increase the conductivity for electrochemical experiments, as well as surface area.

Chemical characterization

NMR spectra were recorded on a 500 MHz spectrometer with UI500NB. NMR sample was prepared with 10-15 mg of polymer in 700 µL solvent. GPC analysis for PFPMAm used the column of PSS NOVEMA Max (5 mm × 50 mm × 5 µm), and NaCl TFA was used as the eluent. Poly(2-vinylpyridine) was used as standard with a sample volume of 50 µL at a flow rate of 1 mL/min. GPC analysis for PFEMA used the column of Tosoh (7.8 mm x 30 cm x 5 µm), and LiBr DMF was used as the eluent. Poly(methyl methacrylate) standards were used for the calibration with the flow rate of 0.6 mL/min. GPC analysis for PFcMA used the column of TSKgel GMHhr-H (7.8 mm x 30 cm x 5 µm), and THF was used as the eluent. Poly(styrene)

standards were used for the calibration with the flow rate of 0.3 mL/min.

Liquid-phase analytics

The concentration of PGMs in the solutions was measured by Inductively Coupled Plasma Optical Emission Spectroscopy (5110 ICP-OES, Agilent Technologies) using an eluent of 5 wt% hydrochloric acid. Samples were diluted with 5 wt% hydrochloric acid and were analyzed with the ICP-OES in 8 replicates. The wavelengths for determining concentration of PGMs and other elements were Pt 214.424 nm, Ir 224.268 nm, Ru 267.876 nm, Pd 340.458 nm, Rh 343.488 nm, Fe 238.204 nm, La 333.749 nm, Sm 359.259 nm, Sc 361.383 nm, Y 371.029 nm, Pr 417.939 nm, and Ce 418.659 nm.

Electrochemical characterization and separation

Cyclic voltammetry (CV) was performed at 20 mV s^{-1} scan rate to evaluate the reversibility of the redox-copolymer and the redox potential. A three-electrode system, with redox polymer-CNT coated carbon paper as working and carbon paper as counter electrodes and Ag/AgCl (3 M KCl) as a reference, was used. The measurements were performed in 2 mL of 20 mM $NaClO_4$ in aqueous solution.

Electrosorption/release and separation factor tests were conducted with 3D-printed electrochemical cells (**Fig. S25, ESI**) as previously reported.[37] The 3-D printed electrochemical cells were constructed with polypropylene with a layer thickness of 0.1 mm and parallel spacing of 1 cm^2 for working and counter electrode with a hole for kinetic sampling. All electrosorption/release and separation factor tests were performed with a 3*1 cm redox polymer-CNT working electrode (1*1 cm coated), a 3*1 cm plain carbon paper counter electrode, an Ag/AgCl reference electrode, and a magnetic stir bar. For electrosorption/release tests, to remove any surface impurities and make sure all redox electrodes were fully reduced, five cycles of cyclic voltammetry from -0.2 to 0.8 V at 20 mV s^{-1} were run in 20 mM $NaClO_4$ solution and stopped at zero current at the end of fifth cycle with BioLogic SP-200 single-channel potentiostat before the electrosorption tests. After that, redox electrodes were transferred to another 3-D printed cell containing 2 mL of 1 mM PGMs anions (H_2IrCl_6, K_3IrCl_6, H_2PtCl_6, Na_3RhCl_6, K_2PdCl_4, $K_2Ru(NO)Cl_5$, Sigma-Aldrich) and 20 mM $NaClO_4$ or NaCl (for K_2PdCl_4 only) in as analytical solution unless otherwise specified. Supporting electrolyte was used to simulate competing anions from waste streams and leachates, and to maintain a more stable conductivity regime for both the adsorption and desorption measurements. Open circuit potential or 0.8 V versus Ag/AgCl were applied onto polymer-CNT electrode for 1 hour for electrosorption unless otherwise specified. Regeneration of polymer-CNT redox electrode was carried out by applying 0.2 V versus Ag/AgCl for 1 hour in a clean 20 mM $NaClO_4$ solution. For kinetic adsorption/release tests, 50 µL aliquots of the solution were retrieved for analysis at different time points.

Separation factors (α) were calculated by the equation below:

$$\alpha_{A,B} = N_{A,ads}/C_{A,sol} \times C_{B,sol}/N_{B,ads}$$

Where $N_{A,ads}$ is the uptake of species A in molar quantity, $N_{B,ads}$ is the uptake of species B in molar quantity, $C_{A,sol}$ is the concentration of species A in the remaining solution, $C_{B,sol}$ is the concentration of species B in the remaining solution. If the separation factor is higher than 1, it means that a redox polymer has higher selectivity toward species A rather than B (indicated by red colored square); if

separation factor is lower than 1, it means that a redox polymer has higher selectivity toward species B rather than A (indicated by blue colored square). The calculation of uptake, regeneration efficiency, and energy consumption can be found in '*SI I. Experimental Procedures, ESI*†.'

Chloralkali electrolysis used same setup as electrosorption tests. For the control chloralkali electrolysis, carbon paper was set as both working and counter electrode and applied constant -100 μA for 15 minutes in 25 wt% NaCl aqueous solution. For chloroalkali electrolysis with PVF-CNT, PVF-CNT was pre-oxidized at 0.8 V versus Ag/AgCl in $NaClO_4$ for 10 minutes then transfer to 25 wt% NaCl aqueous solution and applied -100 μA constant current for 15 minutes.

In-situ electrosorption was carried out using Electrochemical quartz crystal microbalance (EQCM, BioLogic BluQCM QSD (QSD-TCU)) to measure the frequency change with Au-coating 5 MHz quartz crystal, with a piezo electroactive area of 0.2 cm^2 (diameter: 14 mm, polished finish, AW-R5CUP, BioLogic) working electrode, platinum wire counter, and Ag/AgCl (in 3M NaCl) reference electrode. The working electrode was spun coated (2000 rpm for 1 min with acceleration of 1000 rpm) with 50 μL PVF solution (7.5 mg/mL in chloroform) and 1 mM PGMs analyte solution was added to the electrochemical cell before analyzing. The mass change was determined by Sauerbrey equation. The calculation detail can be found in '*SI I. Experimental Procedures, ESI*†.'

Catalytic Converter Recycling

A new catalytic converter from a 2014 Scion Tc was purchased from Toyota, and the internal PGM-coated catalyst material was removed from the stainless-steel tubing with a grinding wheel. 663 g of catalyst material was recovered from the catalytic converter, which was then finely ground with mortar and pestle. In a typical digestion, 1 g of crushed catalyst material was added to 25 mL of 38% hydrochloric acid. Chlorine gas was generated in-situ by adding 5 mL of a 9% sodium hypochlorite solution. The vessel was sealed shut with Teflon tape and left to stir for 24 hours. The solution was filtered and evaporated at 40 °C until only 1 mL of solution remained to remove excess chlorine gas and HCl. Finally, 24 mL of DI water was added to the 1 mL concentrate for a final catalyst digestion solution. The solution was analyzed with ICP-OES, with its composition is shown in Table S1. (ESI†) Adsorption experiments were carried out in a similar manner as previous tests: a PVF-CNT electrode with 0.2 mg of PVF and a 1x1 cm area was placed in 1.5 mL of digested catalyst solution along with Ag/AgCl reference and carbon paper counter electrode. The cell was operated either at open circuit potential or at a constant 0.8 V vs Ag/AgCl for 1 hour.

Conflicts of interest

There are no conflicts to declare.

Acknowledgements

Notes and references

1.   U.S. Department of Energy, Critical Materials Assessment 2023, https://www.energy.gov/sites/default/files/2023-07/doe-critical-material-assessment_07312023.pdf, (accessed August 2023).
2.   M. K. Debe, *Nature*, 2012, **486**, 43-51.
3.   M. F. Li, Z. P. Zhao, T. Cheng, A. Fortunelli, C. Y. Chen, R. Yu, Q. H. Zhang, L. Gu, B. V. Merinov, Z. Y. Lin, E. B. Zhu, T. Yu, Q. Y. Jia, J. H. Guo, L. Zhang, W. A. Goddard, Y. Huang and X. F. Duan, *Science*, 2016, **354**, 1414-1419.
4.   S. Park, Y. Y. Shao, J. Liu and Y. Wang, *Energy Environ. Sci.*, 2012, **5**, 9331-9344.
5.   J. Kaspar, P. Fornasiero and N. Hickey, *Catal. Today*, 2003, **77**, 419-449.
6.   E. Antolini, *ACS Catal.*, 2014, **4**, 1426-1440.
7.   R. Lang, T. B. Li, D. Matsumura, S. Miao, Y. J. Ren, Y. T. Cui, Y. Tan, B. T. Qiao, L. Li, A. Q. Wang, X. D. Wang and T. Zhang, *Angew. Chem.-Int. Edit.*, 2016, **55**, 16054-16058.
8.   C. Y. Zhang, C. Xu, X. Y. Gao and Q. Q. Yao, *Theranostics*, 2022, **12**, 2115-2132.
9.   E. Antolini, *Energy Environ. Sci.*, 2009, **2**, 915-931.
10.   R. R. Adzic, J. Zhang, K. Sasaki, M. B. Vukmirovic, M. Shao, J. X. Wang, A. U. Nilekar, M. Mavrikakis, J. A. Valerio and F. Uribe, *Top. Catal.*, 2007, **46**, 249-262.
11.   Johnson Matthey 2022 PGM market report, https://matthey.com/pgm-market-report-2022, (accessed January 2023).
12.   P. Sinisalo and M. Lundstrom, *Metals*, 2018, **8**, 12.
13.   F. Crundwell, M. Moats, V. Ramachandran, T. Robinson and W. G. Davenport, *Extractive metallurgy of nickel, cobalt and platinum group metals*, Elsevier, 2011.
14.   B. Raju, J. R. Kumar, J. Y. Lee, H. S. Kwonc, M. L. Kantam and B. R. Reddy, *J. Hazard. Mater.*, 2012, **227**, 142-147.
15.   M. Rzelewska-Piekut and M. Regel-Rosocka, *Sep. Purif. Technol.*, 2019, **212**, 791-801.
16.   T. H. Nguyen, C. H. Sonu and M. S. Lee, *Hydrometallurgy*, 2016, **164**, 71-77.
17.   B. J. Glaister and G. M. Mudd, *Miner. Eng.*, 2010, **23**, 438-450.
18.   S. Harjanto, Y. Cao, A. Shibayama, I. Naitoh, T. Nanami, K. Kasahara, Y. Okumura, K. Liu and T. Fujita, *Mater. Trans.*, 2006, **47**, 129-135.
19.   M. Fan, S. L. Li, H. Deng, X. G. Zhang, G. T. Luo, Z. J. Huang and M. H. Chen, *Sep. Purif. Technol.*, 2022, **289**, 11.
20.   S. Ilyas, R. R. Srivastava, H. Kim and H. A. Cheema, *Sep. Purif. Technol.*, 2020, **248**, 8.
21.   A. M. Yousif, *J. Chem.*, 2019, **2019**, 7.
22.   G. Nicol, E. Goosey, D. S. Yildiz, E. Loving, V. T. Nguyen, S. Riano, I. Yakoumis, A. M. Martinez, A. Siriwardana, A. Unzurrunzaga, J. Spooren, T. A. Atia, B. Michielsen, X. Dominguez-Benetton and O. Lanaridi, *Johns. Matthey Technol. Rev.*, 2021, **65**, 127-147.
23.   L. N. Zhang, R. Li, H. Y. Zang, H. Q. Tan, Z. H. Kang, Y. H. Wang and Y. G. Li, *Energy Environ. Sci.*, 2021, **14**, 6191-6210.

24. S. Dresp, F. Dionigi, M. Klingenhof and P. Strasser, *ACS Energy Lett.*, 2019, **4**, 933-942.

25. I. A. Moreno-Hernandez, B. S. Brunschwig and N. S. Lewis, *Energy Environ. Sci.*, 2019, **12**, 1241-1248.

26. D. I. Kim, G. Gwak, P. Dorji, D. He, S. Phuntsho, S. Hong and H. Shon, *ACS Sustain. Chem. Eng.*, 2018, **6**, 1692-1701.

27. R. L. Chen, J. Y. Feng, J. Jeon, T. Sheehan, C. Ruttiger, M. Gallei, D. Shukla and X. Su, *Adv. Funct. Mater.*, 2021, **31**, 11.

28. M. E. Suss, S. Porada, X. Sun, P. M. Biesheuvel, J. Yoon and V. Presser, *Energy Environ. Sci.*, 2015, **8**, 2296-2319.

29. S. E. C. Sener, V. M. Thomas, D. E. Hogan, R. M. Maier, M. Carbajales-Dale, M. D. Barton, T. Karanfil, J. C. Crittenden and G. L. Amy, *ACS Sustain. Chem. Eng.*, 2021, **9**, 11616-11634.

30. G. Lota, K. Fic and E. Frackowiak, *Energy Environ. Sci.*, 2011, **4**, 1592-1605.

31. K. Kim, R. Candeago, G. Rim, D. Raymond, A. H. A. Park and X. Su, *iScience*, 2021, **24**, 31.

32. X. Su, H. J. Kulik, T. F. Jamison and T. A. Hatton, *Adv. Funct. Mater.*, 2016, **26**, 3394-3404.

33. K. Kim, S. Cotty, J. Elbert, R. L. Chen, C. H. Hou and X. Su, *Adv. Mater.*, 2020, **32**, 8.

34. X. Su, K. J. Tan, J. Elbert, C. Ruttiger, M. Gallei, T. F. Jamison and T. A. Hatton, *Energy Environ. Sci.*, 2017, **10**, 1272-1283.

35. H. Vapnik, J. Elbert and X. Su, *J. Mater. Chem. A*, 2021, **9**, 20068-20077.

36. T. H. Nguyen, C. H. Sonu and M. S. Lee, *J. Ind. Eng. Chem.*, 2016, **36**, 245-250.

37. S. Cotty, J. Jeon, J. Elbert, V. S. Jeyaraj, A. V. Mironenko and X. Su, *Sci. Adv.*, 2022, **8**, 12.

38. J. Jeon, J. Elbert, C. H. Chung, J. Chae and X. Su, *Adv. Funct. Mater.*, 2023, DOI: 10.1002/adfm.202301545, 10.

39. B. Y. Kim, E. L. Ratcliff, N. R. Armstrong, T. Kowalewski and J. Pyun, *Langmuir*, 2010, **26**, 2083-2092.

40. N. Kim, J. Elbert, C. Kim and X. Su, *ACS Energy Lett.*, 2023, **8**, 2097-2105.

41. M. L. Hu, M. Abbasi-Azad, B. Habibi, F. Rouhani, H. Moghanni-Bavil-Olyaei, K. G. Liu and A. Morsali, *ChemPlusChem*, 2020, **85**, 2397-2418.

42. A. Paul, R. Borrelli, H. Bouyanfif, S. Gottis and F. Sauvage, *ACS Omega*, 2019, **4**, 14780-14789.

43. M. W. Cooke, T. S. Cameron, K. N. Robertson, J. C. Swarts and M. A. S. Aquino, *Organometallics*, 2002, **21**, 5962-5971.

44. P. O. Schwartz, S. Fortsch, E. Mena-Osteritz, D. Weirather-Kostner, M. Wachtler and P. Bauerle, *RSC Adv.*, 2018, **8**, 14193-14200.

45. A. M. Wilson, P. J. Bailey, P. A. Tasker, J. R. Turkington, R. A. Grant and J. B. Love, *Chem. Soc. Rev.*, 2014, **43**, 123-134.

46. J. L. Wang and X. Guo, *J. Hazard. Mater.*, 2020, **390**, 18.

47. C. M. Woodbridge, D. L. Pugmire, R. C. Johnson, N. M. Boag and M. A. Langell, *J. Phys. Chem. B*, 2000, **104**, 3085-3093.

48. X. Y. Wu, Y. K. Xu, C. Zhang, D. P. Leonard, A. Markir, J. Lu and X. L. Ji, *J. Am. Chem. Soc.*, 2019, **141**, 6338-6344.

49. I. G. Casella, M. Contursi and R. Toniolo, *J. Electroanal. Chem.*, 2015, **736**, 147-152.

50. M. Schnippering, P. R. Unwin, J. Hult, T. Laurila, C. F. Kaminski, J. M. Langridge, R. L. Jones, M. Mazurenka and S. R. Mackenzie, *Electrochem. Commun.*, 2008, **10**, 1827-1830.

51. H. Hübner, R. Candeago, D. Schmitt, A. Schießer, B. Xiong, M. Gallei and X. Su, *Polymer*, 2022, **244**, 124656.

52. R. Chen, H. Wang, M. Doucet, J. F. Browning and X. Su, *JACS Au*, 2023, **3**, 3333-3344.

53. R. Candeago, H. Wang, M.-T. Nguyen, M. Doucet, V.-A. Glezakou, J. F. Browning and X. Su, *JACS Au*, 2024, DOI: 10.1021/jacsau.3c00705.

54. A. J. Bard, L. R. Faulkner and H. S. White, *Electrochemical methods: fundamentals and applications*, John Wiley & Sons, 2022.

55. Y. Gogotsi and P. Simon, *Science*, 2011, **334**, 917-918.

56. R. Prins, A. R. Korswagen and A. G. Kortbeek, *J. Organomet. Chem.*, 1972, **39**, 335-+.